ACS OMEGA

Open Access

http://pubs.acs.org/journal/acsodf

Article

Phytosynthesized Iron Oxide Nanoparticles Using Aqueous Extract of *Saccharum arundinaceum* (Hardy Sugar Cane), Their Characterizations, Antiglycation, and Cytotoxic Activities

Published as part of the ACS Omega virtual special issue "Phytochemistry".

Saeed M Aldossari, Latif Ur Rehman, Ijaz Ahmad,* Madeeha Aslam, Fozia Fozia,* Mohamed Mohany, Marija Milošević, Salim S. Al-Rejaie, and Mourad A. M. Aboul-Soud

Cite This: *ACS Omega* 2023, 8, 41214−41222

Read Online

ACCESS | Metrics & More | Article Recommendations

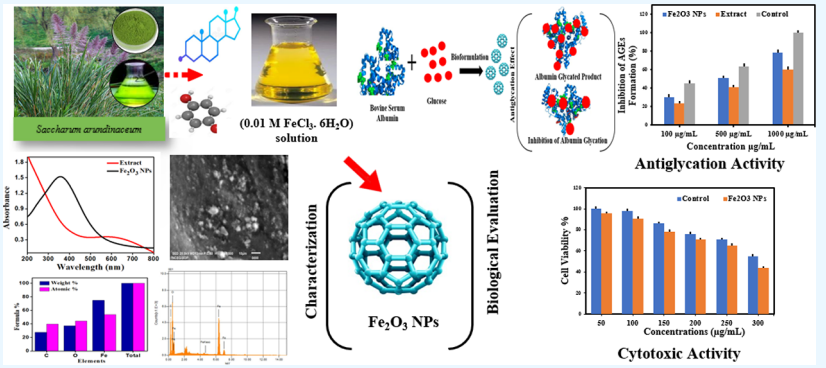

ABSTRACT: The goal of the current study is to achieve plant-mediated synthesis of iron oxide nanoparticles (Fe_2O_3 NPs). The plant extract of *Saccharum arundinaceum* was used as a reducing and stabilizing agent for the synthesis of Fe_2O_3 NPs. Different techniques such as energy-dispersive X-ray analysis (EDX), X-ray diffraction (XRD), scanning electron microscopy (SEM), Fourier-transform infrared spectroscopy (FT-IR), and UV−visible spectroscopy (UV−vis) were used to characterize the synthesis of Fe_2O_3 NPs. UV−visible spectroscopy verified the synthesis of Fe_2O_3 NPs using a surface plasmon resonance peak at a wavelength of 370 nm. SEM analysis specifies the spherical morphology of the synthesized nanoparticles with a size range between 30 and 70 nm. The reducing and capping materials of Fe_2O_3 NPs were revealed by FT-IR analysis based on functional group identification. The plant extract contained essential functional groups, such as C−H, C−O, N−H, $-CH_2$, and −OH, that facilitate the green synthesis of Fe_2O_3 NPs. The EDX analysis detected the atomic percentage with the elemental composition of Fe_2O_3 NPs, while the XRD pattern demonstrated the crystallinity of Fe_2O_3 NPs. Furthermore, the synthesized Fe_2O_3 NPs showed potential antiglycation activity under *in vitro* conditions, which was confirmed by the efficient zone of inhibition on glycation of bovine serum albumin/glucose (BSA-glucose) in the order <100 < 500 < 1000 μg/mL, which revealed that Fe_2O_3 NPs showed significant antiglycation activity. Additionally, the cytotoxic activity against brain glioblastoma cells was assessed using the MTT assay, which exhibited diminished cytotoxic activity at concentrations lower than 300 μg/mL. Thus, we assumed that the resulting Fe_2O_3 NPs are a good option for use in drug delivery and cancer treatments.

1. INTRODUCTION

Metallic nanoparticles are incredibly interesting because they exhibit greater thermal conductivity than fluids in the solid forms. Among metallic nanoparticles, ferromagnetic nanoparticles are inherently magnetic, in contrast to stable noble metals, such as platinum, gold, silver, and palladium. Typically, ferromagnetic components of magnetic nanoparticles are nickel, cobalt, and iron. Fe_2O_3 NPs with various polymorph forms have substantial exploration due to their ubiquitous use in modern science and technological innovation.[1] Fe_2O_3 NPs have been extensively used in biomedicine as a drug delivery system due to their characteristic properties including nanoscale zerovalent iron (nZVI/Fe0), low toxicity, super-

Received: June 23, 2023
Revised: September 17, 2023
Accepted: October 4, 2023
Published: October 23, 2023

paramagnetism, and high surface area to volume ratios. The exclusive physical and chemical properties of Fe_2O_3 NPs (chemical and magnetic stability) can help them to remain attached to tissues for a long time, avoiding the effects of oral and intravenous administration.[2−4] Although several chemical and physical approaches are most widely used for the synthesis of Fe_2O_3 NPs, most of these methods involve the use of poisonous chemicals, produce hazardous byproducts, require extreme chemical conditions, and use chemically contaminated precursors, which substantially limit the biomedical applications, especially in the field of medicine.[5] Therefore, in order to broaden the scope of Fe_2O_3 NPs in biomedical applications including cosmetics, bioremediation, biomedicine, and diagnostic and materials engineering,[6] it is crucial to identify nontoxic, environmentally friendly, and stable procedures for the synthesis of Fe_2O_3 NPs. The use of nontoxic chemicals, eco-friendly methods, and organic materials are thought to be the main factors that contribute to green source synthesis of Fe_2O_3 NPs.[7] One of the key issues is to select the significant reducing agent that is responsible for the synthesis of superparamagnetic Fe_2O_3 NPs by using the green synthesis procedure, which exhibits small band gap energy, has a large surface area, and is highly stable in nature. Thus, the green synthesis of Fe_2O_3 NPs is cost-effective, nontoxic, and eco-friendly, being synthesized using different medicinal plants.[8] This implies that the green method for the Fe_2O_3 NP synthesis offers more advantages than the chemical and physical approaches, which contributes to alleviating the concerns associated with these approaches. Recent studies clarify that the plant extracts of *Parthenium hysterophorus*,[9] *Ruellia tuberosa*,[10] and *Nephrolepis exaltata*[11] were used for the synthesis of Fe_2O_3 NPs.

Furthermore, the plant extract was also found to exhibit an inhibitory effect on glycation to decrease the blood glucose level and α-glucosidase in normal and diabetic patients. Glycation is a spontaneous, nonenzymatic interaction between free amino groups, free reducing sugars of proteins, lipids, and DNA that leads to Amadori products. The Amadori products undergo a variety of irreversible dehydration and rearrangement instances, resulting in the development of advanced glycation end products (AGEs).[12] Glycation impairs the flexibility of tissues like skin, blood vessels, and tendons and causes proteins to lose their function.[13] Several NSAIDs (nonsteroidal anti-inflammatory medicines), including nimesulide, meloxicam, mefenamic acid, piroxicam, and oxaprozin, were assessed for their antiglycation activity.[14] Due to the resistance of these drugs, nanoparticles (NPs) could be an alternative drug used against glycation. The antiglycation activities of gold nanoparticles synthesized by *Labisia pumila* extract and silver nanoparticles synthesized by using *Rosa damascena* flower extract have also been reported.[15,16] Thus, we can say that the medicinal plant-mediated NPs might be useful for the treatment of glycation. Therefore, the plant-mediated synthesis is necessary to synthesize Fe_2O_3 NPs and possesses diverse biological potential that might be effective against glycation and hence can be detected as a key source for antiglycation activity.

So, the current work aims to synthesize Fe_2O_3 NPs using plant extract of *Saccharum arundinaceum* that serves as a reducing and stabilizing agent. The extensive study revealed that *Saccharum arundinaceum* plant extract was not reported for the synthesis of Fe_2O_3 NPs. Therefore, the synthesis of Fe_2O_3 NPs was achieved using an aqueous plant extract of *Saccharum arundinaceum*, and then, we investigate the antiglycation and cytotoxic activities that were not reported earlier in the literature; we are reporting it for the first time. The plant *Saccharum arundinaceum* is a wild species of *Saccharum officinarum* and is commonly known as sugar cane, which is a native species of grass that has been discovered in various locations used for the dumping of distillery sludge in India. It is a type of perennial grass that is only found in the tropical South and Southeast Asia. In addition to having strong tillering capability, *Saccharum arundinaceum* has a high resistance to pests, drought, diseases, cold, and infertile soils. Sugar cane has been used all over the world to cure a wide range of illnesses and is also employed in the Ayurvedic medical system as a single medicament or in combination with other substances from plants.[17] However, the phytoconstituents contain bioreductants and stabilizers including tricin and apigenin, luteoline glycosides, flavonoids such as vitexin, orientin, swertisin, policosanols, and schaftoside, and steroids that serve as the major phytochemicals in sugar cane.[18] Because of these phytochemical components and bioactivities, it has been observed in recent years that a lot of attention has been paid to the investigation of potential treatments for various diseases.[19] Therefore, the goal of the current study was to achieve the synthesis of Fe_2O_3 NPs using *Saccharum arundinaceum* plant extract and to explore its antiglycation and cytotoxic activities. Moreover, the synthesized Fe_2O_3 NPs were carried out under different techniques, including EDX, XRD, SEM, FT-IR, and UV−vis spectrophotometry, that were used to analyze the geometry, elemental composition, and optical and morphological properties of NPs. Further, the zone of inhibition activity of synthesized Fe_2O_3 NPs against AGE products and the MTT assay were used to evaluate the cytotoxic activity.

2. MATERIALS AND METHODS

2.1. Chemicals. The chemical ferric chloride hexahydrate ($FeCl_3{\cdot}6H_2O$) was purchased from Sigma-Aldrich (USA). Analytical-grade ethanol, glucose, BSA, trichloroacetic acid (TCA), aminoguanidine, and doxorubicin were purchased from Merck (Germany). Further, (3-(4,5-dimethylthiazole-2-yl)-2,5-diphenyl tetrazolium (Sigma-Aldrich, USA) and dimethyl sulfoxide (DMSO) were used in the MTT assay.

2.2. Preparation of Plant Extract. The fresh *Saccharum arundinaceum* plant was harvested from the hilly regions of District Karak in Khyber Pakhtunkhwa, Pakistan. The plant was authenticated at the Department of Botanical and Environmental Sciences, Kohat University of Science & Technology, Kohat, Pakistan, where a voucher specimen (no. Bot-KUST-1575) was preserved in the herbarium. The whole plant was surface cleansed with tap water to remove dirt and other impurities. After that, it was cleaned with distilled water and allowed to air-dry at room temperature in the shade. A beaker containing 20 g of finely chopped plant material and 200 mL of distilled water was heated at 40 °C for 30 min. The extract was cooled before being filtered using Whatman filter paper no. 1 and was kept in a refrigerator that was used for the synthesis of Fe_2O_3 NPs.

2.3. Green Synthesis of Fe_2O_3 NPs. The synthesis of Fe_2O_3 NPs was carried out by a green synthesis procedure. In this experiment, 10 mL of an aqueous solution of 0.01 M $FeCl_3{\cdot}6H_2O$ was mixed into 70 mL of *Saccharum arundinaceum* plant extract. The reaction mixture was continuously stirred at 200 rpm for 2 h at pH 10 and a temperature of 70 °C, in a

https://doi.org/10.1021/acsomega.3c04484
ACS Omega 2023, 8, 41214−41222

rotatory orbital shaker. As a result, the color of the solution changed from pale yellow to dark brown, signifying the synthesis of NPs. The synthesized Fe_2O_3 NPs were further examined under a UV−vis spectrophotometer to validate the synthesis. After that, the Fe_2O_3 NPs were isolated to centrifuge the reaction mixture for 20 min at 6000 rpm. The precipitates were collected by washing up to three times using distilled water and ethanol to remove the impurities. The Fe_2O_3 NPs were dried at 40 °C under vacuum to attain the powder NPs that were further used for characterizations and biomedical screening.[9]

2.4. Characterization of Fe_2O_3 NPs. The synthesis of Fe_2O_3 NPs was identified by using various techniques, including EDX, SEM, XRD, FT-IR, and UV−vis spectroscopy.

2.4.1. UV−Vis Spectroscopy. A UV−vis spectrophotometer can be used to conveniently detect the synthesis of Fe_2O_3 NP solution from plant extract. UV−vis analysis was able to monitor the bioreduction of the Fe ions in solutions by periodically sampling aliquots (1 mL) of the aqueous solution to get an idea of the SPR of the UV−vis spectrum. A spectrophotometer scanning in the 400−600 nm region with a resolution of 1 nm was used to monitor the UV−vis spectra of these aliquots as a function of the reaction time.

2.4.2. FT-IR Analysis. The presence of biomolecules and the interaction of the green synthesized Fe_2O_3 NPs with the capping agent were discovered using FT-IR analysis. An FT-IR (Thermo Scientific) spectrophotometer was used to perform the measurements on air-dried iron oxide NPs at a resolution of 4 cm^{-1} at the wavenumber range of 500−3500 cm^{-1}.

2.4.3. XRD Analysis. The crystalline nature and particle size of the synthesized NPs were determined by using XRD patterns. In the experiment, a Shimadzu XRD-6000/6100 model with 30 mA, 30 keV, and Cu Kα radiation at a 2θ angle was used. A rapid analytical method that can be used to determine the crystalline phase of NPs and the size of individual unit cells is X-ray powder diffraction.

2.4.4. SEM Analysis. SEM is a particular kind of electron microscope that creates an image of samples with high-energy electron beams by the use of raster-scanning. A JEOL model 6390 microscope was used for analyzing the SEM images. SEM samples were prepared by diluting the sample at 10 mg/L suspensions of NPs followed by drying the drop of samples that was simply dropped on the SEM grid. The remaining solution was wiped off using blotting paper, and then, the SEM grid was exposed to a mercury lamp for 5 min to dry the thin films. In order to prevent charging, the NPs were put on a carbon-coated SEM grid along with gold-coated sputtering used to analyze the results of SEM at a 30 keV accelerating voltage.

2.4.5. EDX Analysis. EDX analysis was used to detect the elemental composition of synthesized Fe_2O_3 NPs by using a scanning electron microscope. Upon collision with the electron beam in typical SEM, the samples interact with the beam and produce characteristic X-rays. The X-ray is the result of the primary beam of electron interaction with the nucleus of the sample atom. The electron is excited from the outer shell of the atom to the missing ejected electron and releases the X-ray. These characteristic X-rays were recorded by an energy-dispersive spectrometer for the measurement of the elemental composition in the NPs at 20 keV.

2.5. Antiglycation Analysis. To examine the effect of plant extract and Fe_2O_3 NPs on the nonenzymatic glycosylation process, AGE albumin was obtained by mixing 500 mL of BSA with 400 mL of glucose, along with different quantities of extract and Fe_2O_3 NPs (100, 500, and 1000 μg/mL), in a 0.2 mM phosphate buffer pH 10 solution. After that, 10 μL of trichloroacetic acid (TCA) was mixed into the reaction mixture and then allowed to proceed at 60 °C for 72 h. The mixture containing TCA was then centrifuged at 6000 rpm for 10 min at a temperature of 40 °C. The reaction mixture was incubated for 21 days at room temperature. The fluorescence intensity of the samples (total AGE level) was calculated after the incubation period using a micro titer-plate multimode detector with maximal emission wavelengths at 370 and 440 nm. Aminoguanidine was included as the control group. The relative quantity of glycated BSA-glucose was identified by using the emission and excitation wavelengths of spectrophotometry.[16]

2.6. Cytotoxic Activity of Fe_2O_3 NPs. The *in vitro* cytotoxicity of green synthesized Fe_2O_3 NPs on brain tumor cells (U87) was examined using the MTT assay.[20] In order to achieve a confluence of around 70−90%, a number of cells (5×10^3) were distributed into each well of a 96-well microplate and were incubated at 37 °C in a humidified atmosphere with 5% CO_2 and 95% air. Each well received 50 μL of NPs, which was then incubated at 37 °C for 24 h. The medium was then removed, and 100 μL of phosphate-buffered saline was used to wash the wells twice for 2−3 min. After that, 20 μL of MTT (3-(4,5-dimethylthiazole-2-yl)-2,5-diphenyl tetrazolium, Sigma-Aldrich, USA) stock solution was added to each well, and the wells were then incubated at 37 °C for 4 h in a humidified atmosphere, 5% CO_2 and 95% air. The resultant formazan was dissolved by adding 100 μL of DMSO to each well. In the final stage, adsorption was measured by using an ELISA reader (model 50, Bio-Rad Corp., Hercules, CA) operating at a 570 nm wavelength. The standard drug doxorubicin was used as the control group. Additionally, the following equation (eq 1) was used to determine the percentage of cell viability (survival):

$$\text{cell viability}(\%) = [100 \times (\text{sample abs})/(\text{control abs})] \quad (1)$$

where the cell viability corresponds to %, absorption of the test group is represented by (sample abs), and the absorption of the control group is denoted by (control abs).

2.7. Statistical Analysis. The results were calculated as the mean standard deviation (n = 3). The obtained data were statistically performed using t tests with GraphPad Prism version 10.0.1. The analysis of variance using t tests was within the significance of $P < 0.05$.

3. RESULTS AND DISCUSSION

3.1. UV−Visible Analysis of Fe_2O_3 NPs. The plant extract of *Saccharum arundinaceum* reports several phytoconstituents including tricin and apigenin and luteoline glycosides such as vitexin, orientin, policosanols, swertisin, schaftoside, and steroids.[18] The synthesis of Fe_2O_3 NPs or the reduction of metallic salts to NPs is caused by these phytoconstituents. They also serve as stabilizing agents that prevent the agglomeration of green synthesized Fe_2O_3 NPs. When the plant extract is mixed into the aqueous solution of salt precursor, the color of the reaction mixture changes from light yellow to a dark brown signifying the formation of Fe_2O_3 NPs. This is due to the fact that the plant extract from *Saccharum arundinaceum* may be able to reduce Fe^{3+} to Fe^0. The organic components of the plant extract react with the Fe ions to form

https://doi.org/10.1021/acsomega.3c04484
ACS Omega 2023, 8, 41214−41222

Fe_2O_3 NPs; this is because first-row transition metals are more prone to oxidation.[21] The formation of Fe_2O_3 NPs was further explained by measuring the absorbance within the range of 200 to 800 nm using a UV−vis spectrophotometer. The sharp SPR formed owing to their shape, particle size, the dielectric of the surrounding medium, and the aggregation state of the NPs. Figure 1 shows the synthesis of Fe_2O_3 NPs under the UV−vis

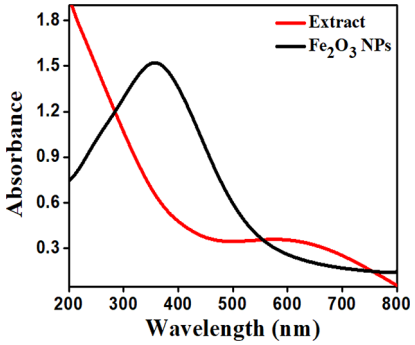

Figure 1. UV−visible spectra of synthesized Fe_2O_3 NPs.

absorption spectra at a concentration of 10 mL of an aqueous 0.01 M $FeCl_3{\cdot}6H_2O$ solution to 70 mL of the *Saccharum arundinaceum* plant extract. The collective oscillation of free electrons in the conduction band of Fe_2O_3 NPs gives rise to the sharp SPR peak.[22] Figure 1 illustrates a comparison between the UV−vis spectra of Fe_2O_3 NPs and the pure *Saccharum arundinaceum* plant extract, which shows that the *Saccharum arundinaceum* plant extracts did not reveal any visible peak. After the interaction of Fe solution to *Saccharum arundinaceum* plant extracts, a visible absorption peak at a wavelength of 370 nm is shown, proving that the plant extract serves as capping and reducing agents that synthesize Fe_2O_3 NPs.

3.2. FT-IR Analysis of Fe_2O_3 NPs. The synthesized Fe_2O_3 NPs and the *Saccharum arundinaceum* plant extract were examined using FT-IR analysis in order to examine the potential alternation to the functional group bonds that may have formed during the reduction process. In the FT-IR spectrum, the *Saccharum arundinaceum* plant extracts showed a number of prominent bands at wavenumbers of 1012, 1253, 1573, 1754, 2996, and 3448 cm^{-1}. Similarly, the synthesized Fe_2O_3 NPs exhibited an extremely comparable pattern. The synthesis of Fe_2O_3 NPs was confirmed by the absorption bands detected at around 887, 786, and 538 cm^{-1}, corresponding to the Fe−O stretching vibration of Fe_2O_3 NPs (Figure 2).[23] In the plant extract, the bands at 1012 and 1253 cm^{-1} correlate to the stretch vibration of C−H and C−O functional groups of amide ($-CH\text{-}NH_2$) and ester (−C−O-C−), respectively.[24] The sharp band at 1573 cm^{-1} represents the symmetric vibration of the N−H amino acid functional group found in plant extract. The carbonyl group indicated by the absorption peak at 1754 cm^{-1} corresponds to the stretching vibration of the C═O bond that stabilized and served as a capping agent. The band at 2996 cm^{-1} might be caused by a stretching vibration of $-CH_2$ aliphatic hydrocarbons.[25] The absorption peak observed at 3448 cm^{-1} corresponds to the stretching vibration of the −OH bond of the polyphenolic functional group. Once the Fe_2O_3 NPs had been reduced, peak shifting was observed. So, the current results revealed that Fe ions were reduced to Fe_2O_3 NPs via the action of polyphenolic, alkane,

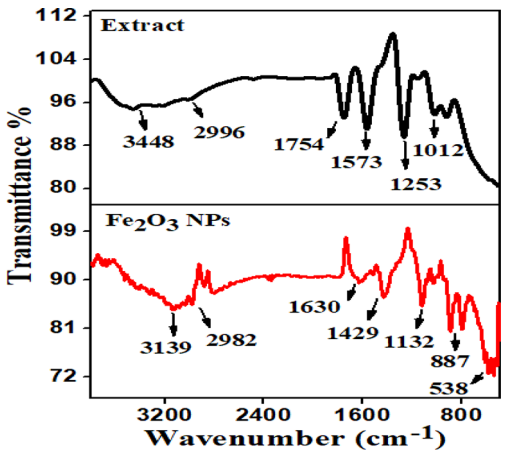

Figure 2. FT-IR spectra of synthesized Fe_2O_3 NPs and aqueous plant extract.

and amino groups.[26] A water-soluble polyphenol compound coated the surface of the synthesized Fe_2O_3 NPs, as indicated by the band with a higher intensity attributed to the −OH groups. It is worth mentioning that the band shifting in the FT-IR analysis revealed that the extract contains biomolecules that were responsible for the synthesis of Fe_2O_3 NPs.

3.3. XRD Pattern of Fe_2O_3 NPs. The XRD patterns examined the phase purity in iron oxide nanoparticles that confirm the crystal structure by using a diffraction pattern. Figure 3 displays the XRD pattern of Fe_2O_3 NPs synthesized

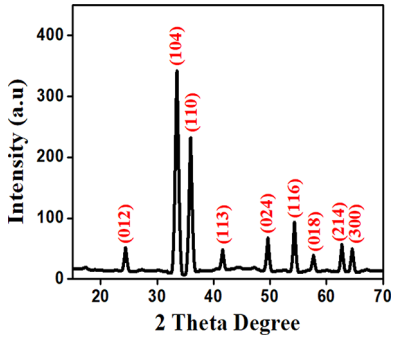

Figure 3. XRD pattern of synthesized Fe_2O_3 NPs.

employing an extract of plant *Saccharum arundinaceum*. The X-ray diffraction pattern has nine distinctive peaks at 23, 33, 36, 42, 49, 54, 58, 63, and 64°, respectively, as indicated by their indices of the (012), (104), (110), (113), (024), (116), (018), (214), and (300) planes at the 2θ degree. These crystal peaks almost exactly resemble the orthorhombic structure. The results match the JCPDS 76-0958 standardized XRD pattern.[27] The Fe_2O_3 NPs made using the *Saccharum arundinaceum* extract were clearly crystalline based on the XRD data. The Debye−Scherrer formula (eq 2) was employed to calculate the average size of the Fe_2O_3 NPs.

$$D = 0.9\lambda/\beta \cos\theta \quad (2)$$

where "λ" denotes the wavelength of the X-ray, fwhm in radians is β, and "θ" represents the diffraction angles. The mean particle size was found to be 32 nm and was determined by the high-intensity peak.

3.4. SEM Analysis of Fe_2O_3 NPs. The morphology and size of the Fe_2O_3 NPs were examined by SEM analysis. The

https://doi.org/10.1021/acsomega.3c04484
ACS Omega 2023, 8, 41214−41222

morphological structure of synthesized NPs is shown in Figure 4. The study revealed that the particle size was in the range of

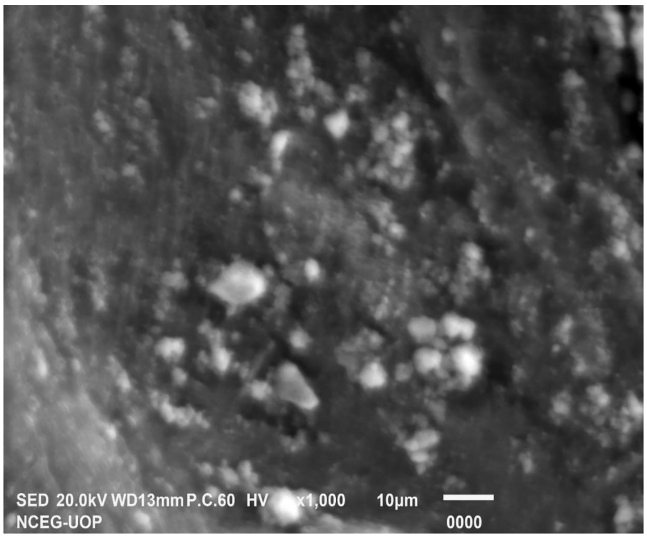

Figure 4. SEM image of synthesized Fe_2O_3 NPs.

30−70 nm, and a similar phenomenon was reported in the previous study.[28] Figure 4 shows that the synthesized Fe_2O_3 NPs were nonuniform, roughly spherical, and in an agglomerated form. The results revealed that large agglomerated clusters were formed due to the magnetic interactions of iron-based NPs, the accumulation of tiny building blocks of various bioactive reducing agents in plant extract, or the minimum capping ability of plant extract. The occurrence of phytoconstituents on the surface of NPs caused the agglomeration.[29] Similarly, Kuang et al. investigated synthesized Fe_2O_3 NPs using three different tea extracts, such as green tea, oolong tea, and black tea. The result showed the irregular spherically shaped Fe_2O_3 NPs.[30]

3.5. Energy-Dispersive X-ray (EDX) Analysis of Synthesized Fe_2O_3 NPs. The elemental composition of Fe_2O_3 NPs was determined by EDX analysis, as shown in Figure 5. The synthesis of Fe_2O_3 NPs was confirmed by the peaks of Fe at 0.7 and 6.4 keV with a standard weight percent of Fe of 76.79%. The result is shown in Figure 5, which revealed that the formation of Fe_2O_3 NPs was confirmed by the peaks of oxygen (O) and iron (Fe). Meanwhile, the absorbance peak of residual C was observed at 0.28 keV in the EDX analysis, which was probably brought about by the X-ray stimulation of the SEM grid and the utilized precursor salt. Similarly, Bharathi et al. demonstrated that the absorbance peaks of C, Na, and S in the EDX spectrum were most possibly due to the excitation of X-rays from used precursor salt and SEM grid.[31] Recently, Behera et al. reported similar findings, which suggests the green synthesis of Fe_2O_3 NPs owned both by Fe and O components that were consistent with results of the current investigation.[29]

3.6. Factor Affecting Stability of Fe_2O_3 NPs. The stability of synthesized Fe_2O_3 NPs was examined by changing the pH and temperature of the reaction mixture. The pH parameter was necessary to recognize the electrical charges carried on biomolecules and may have an impact on the stability as well as the synthesis of NPs. The pH impact on Fe_2O_3 NPs was observed at the pH range of 2−12, as shown in Figure 6A. The absorbance peak of the Fe_2O_3 NP solution did not exhibit any visible peak at a lower pH. However, the shorter-wavelength absorption peaks were observed (the peak shifts more to the left) with the increase of pH (4, 6, 8, and 10). Hence, Figure 6A demonstrates the position of the absorbance peak, and the absorbance intensity of SPR of Fe_2O_3 NPs changed by changing the pH to get the shorter

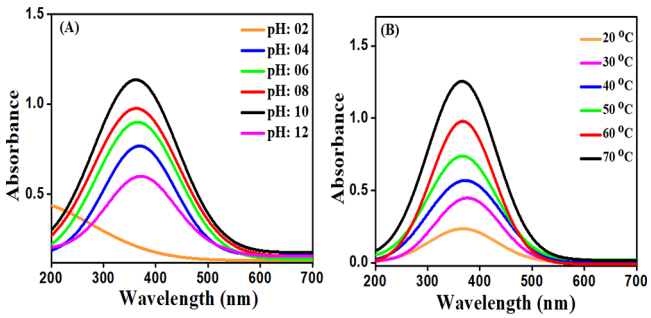

Figure 6. UV−vis spectra of (A) stability of Fe_2O_3 NPs at different pH values (2−12) and (B) temperatures (20−70 °C).

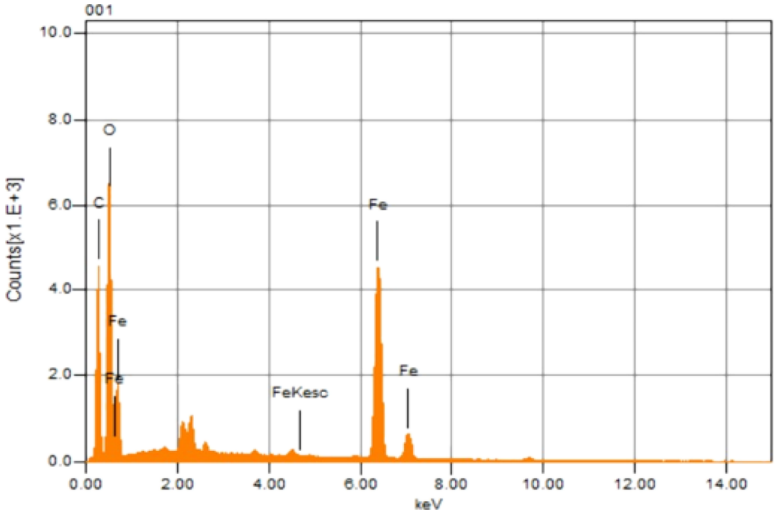

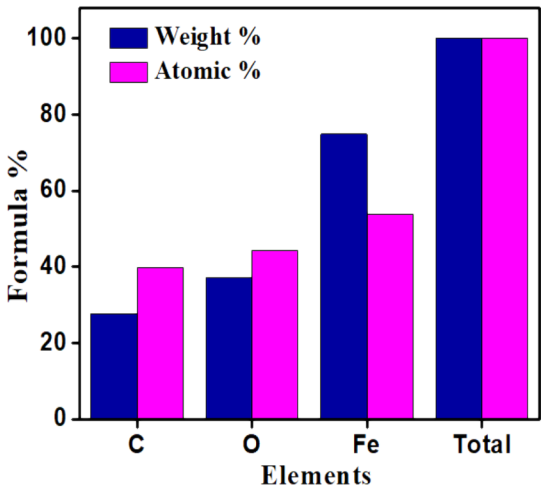

Figure 5. EDX analysis for Fe_2O_3 NPs.

https://doi.org/10.1021/acsomega.3c04484
ACS Omega 2023, 8, 41214−41222

Scheme 1. Proposed Mechanism for the synthesis of Fe_2O_3 NPs

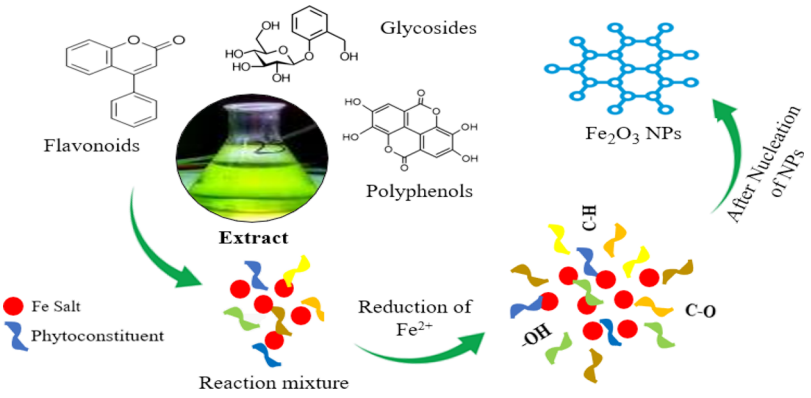

wavelength, which had a small particle size with perfect absorbance intensity. The optimum condition for synthesized Fe_2O_3 NPs was at pH 10; beyond this, the peak intensity becomes lower and shifts toward lower wavelengths.

The stable synthesis of Fe_2O_3 NPs was also influenced by changing the temperature of the reaction mixture from 20 to 70 °C. The absorbance of SPR of Fe_2O_3 NPs is shown in Figure 6B. It was observed that the SPR peak shifts toward a higher absorbance peak by increasing temperature. The synthesis of Fe_2O_3 NPs more easily happens when the temperature is higher than 30 °C. So, the optimum condition for synthesized Fe_2O_3 NPs is at 70 °C that shows a shorter wavelength with perfect absorbance intensity observed in Figure 6B. Therefore, the wavelength of 370 nm was selected as an optimum SPR peak at a 70 °C temperature and pH 10 for the synthesis of Fe_2O_3 NPs.[32]

3.7. Mechanism for Fe_2O_3 NPs Synthesis. Initially, the addition of a salt precursor to a plant extract containing phytochemicals may result in a decrease in ion reduction as well as the stability of NPs. According to the literature, the *Saccharum arundinaceum* plant extract contains various biomolecules including glycosides, polyphenols, flavonoids such as vitexin, orientin, swertisin, policosanols, and schaftoside, and steroids that act as stabilizing and reducing agents.[18] Typically, the −OH group is detected in plant extracts that belong to the polyphenolic group. The −OH groups of polyphenolic compounds are capable of taking part in redox reactions and may reduce Fe ions to Fe_2O_3 NPs. In this case, the polyphenols present in the extract absorb Fe^{2+} and reduce it to Fe^0 and act as a reducing agent.[33] The synthesis of Fe_2O_3 NPs was achieved when Fe ions were reduced by phytochemicals present in the plant extract. The phytochemicals in plant extract with the functional groups, such as C−H, C−O, N−H, $-CH_2$, and −OH, participate on the surface of NPs for stable synthesis of Fe_2O_3 NPs.[34] These groups attach to the surface of Fe_2O_3 NPs and alter their form, growth, and aggregation.[35] Finally, the highly crystalline Fe_2O_3 NPs were synthesized, as shown in Scheme 1.

3.8. Antiglycation Activity. The measurement of antiglycation activity over the duration of the experiment under the incubation period was used to quantify the overall amount of AGE products. The inhibition zones of plant extract and Fe_2O_3 NPs were examined in Figure 7. It was noticed that when the concentration of Fe_2O_3 NPs increases, the inhibitory effect become active. The extract and the Fe_2O_3 NPs showed 60.3 and 78.5% zones of inhibition, which showed the greatest inhibitory effect at 1000 μg/mL concentrations, respectively.

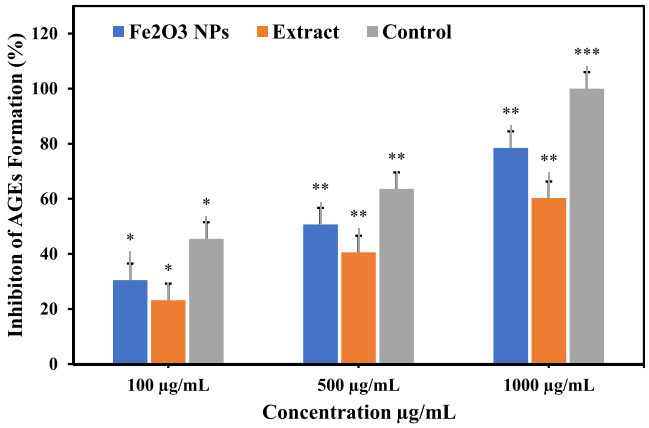

Figure 7. Percentage inhibition of AGE formation in the BSA-glucose system using different concentrations of Fe_2O_3 NPs, extract, and control. *Aminoguanidine was considered as a control group. Results are reported in comparison with the control group. *p values of Fe_2O_3 NPs at concentrations starting from 100 μg/mL are 0.408248, 0.329983, and 0.374166, while the *p values for extract at concentrations starting from 100 μg/mL are 0.163299, 0.410961, and 0.410961. Similarly, the *p values for the control are 0.339935, 0.489898, and 0.08165, respectively.

The formation of AGE products was found to decrease when the concentration of Fe_2O_3 NPs was increased following 100, 500, and 1000 μg/mL. In general, plant extract at various concentrations showed moderate inhibitory effects in contrast to Fe_2O_3 NPs (Figure 7). It appears that nonenzymatic glycosylation of plasma proteins leads to the generation of AGE products during hyperglycemia. The loss of the protein's normal activity, the production of free radicals, the modification in binding of drugs present in plasma, poor fibrinolysis, impairment in the immune system, and platelet activation are only a few of the harmful impacts that it causes.[36] In this work, we examined the significant zone of inhibition of the plant extract and Fe_2O_3 NPs against the development of AGE products. The AGE compound production was inhibited, and blood glucose levels were decreased by both plant extract and Fe_2O_3 NPs. The antiglycation activity of the synthesized Fe_2O_3 NPs was often greater than that of the plant extract. The doses have the best inhibitory impact on albumin glycation at concentrations of 1000 μg/mL. Therefore, the blood glucose effects have been reduced, and the development of AGE compounds has been stopped by both the plant extract and the Fe_2O_3 NPs. It can be concluded that the plant-mediated Fe_2O_3 NPs were very

https://doi.org/10.1021/acsomega.3c04484
ACS Omega 2023, 8, 41214−41222

essential on inhibiting the growth of AGE products.[37] Similarly, Peron and colleagues synthesized silver nanoparticles from the pink *Rosa damascena* plant and have used them to minimize the effects of glucose levels and prevent the production of AGE products.[16] A recent study reports that flavones exhibit stronger inhibitory effects on AGE products with respect to flavanones, flavonols, and isoflavones.[38]

3.9. Biocompatibility Assessment. *3.8.1. Cytotoxicity Results.* In this analysis, the MTT assay was used to assess the cytotoxicity of green synthesized Fe_2O_3 NPs on the brain tumor cell line U87. The test was carried out using NPs with a concentration range of 50−300 μg/mL over a 12 h period (Figure 8). The result of cytotoxic activity suggests that the

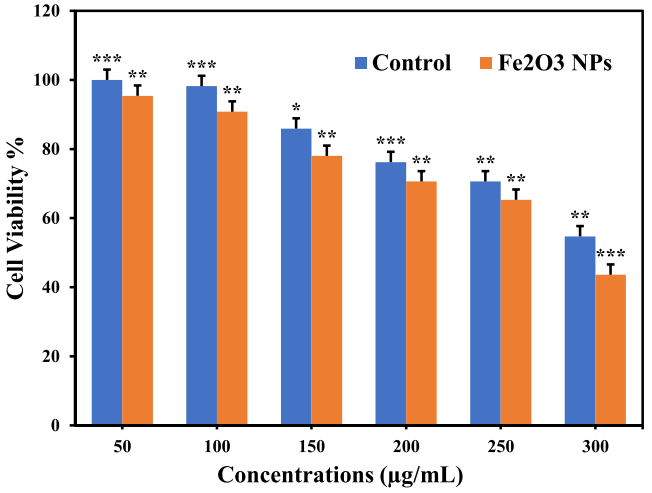

Figure 8. % Cell viability of Fe_2O_3 NPs at different concentrations. *Doxorubicin was considered as a control group. Results are reported in comparison with the control group. *p values of Fe_2O_3 NPs at concentrations starting from 50 μg/mL are 0.249443, 0.374165, 0.35593, 0.244949, 0.244956, and 0.124721. Similarly, the *p values for the control are 0.163299, 0.169967, 0.489923, 0.162345, 0.326613, and 0.243451, respectively.

green synthesized Fe_2O_3 NPs depend on particle size and concentration, which were inactive at concentrations lower than 300 μg/mL. The significant cytotoxic effects were also induced by the use of doxorubicin at a greater concentration. Similarly, Ankamwar et al. demonstrated on cell lines of different types of cancer, and the study revealed that Fe_2O_3 NPs did not show any cytotoxic effects at concentrations below 100 μg/mL.[39] The current investigation is also supported by Izadiyan et al.'s findings, which revealed that green synthesized Fe_2O_3 NPs at various concentrations did not exhibit detectable toxicity to normal cell lines.[40] NPs may result from the phytochemicals and bioactive substances present in the plant extract, which are essential for the capping, stabilization, and synthesis of Fe_2O_3 NPs. The antioxidants and polyphenols prevent the nanoparticles from aggregating and oxidizing and even eliminate the harmful effects of synthesized Fe_2O_3 NPs. Therefore, the use of green synthesized nanoparticles for drug administration and cancer treatment has been suggested because of their strong magnetic and nontoxic characteristics.[41]

4. CONCLUSIONS

In this study, Fe_2O_3 NPs were synthesized using an aqueous extract of *Saccharum arundinaceum* in an affordable, quick, and environmentally friendly manner. The synthesized Fe_2O_3 NPs were examined by FTI-R, UV−vis, SEM, XRD, and EDX techniques. The FT-IR analysis revealed that active biomolecules might have been involved in the reduction of Fe ions that form Fe_2O_3 NPs. The SEM analysis of Fe_2O_3 NPs identifies an average particle size range of 30−70 nm. So, the small particle size indicates good biomedical applications. Moreover, the antiglycation activity of Fe_2O_3 NPs was examined by minimizing the effects of the blood glucose level and preventing the production of AGE compounds. However, the green synthesized Fe_2O_3 NPs did not exhibit toxicity toward the U87 cell line. Thus, Fe_2O_3 NPs were consequently suggested as useful in biomedical industries. In addition, we recommend that further research be conducted on the mechanisms of antiglycation activity and the prevention of metal-catalyzed oxidative destruction of either glucose or other glycated protein intermediates. As a result, antiglycation therapy will be a successful technique in the future to control late diabetes problems by preventing the formation of AGEs.

■ ASSOCIATED CONTENT

Data Availability Statement

The data are available from the corresponding author on reasonable request.

■ AUTHOR INFORMATION

Corresponding Authors

Ijaz Ahmad − *Department of Chemistry, Kohat University of Science & Technology, Kohat 26000, Pakistan;* orcid.org/0000-0002-9139-1611; Email: drijaz_chem@yahoo.com

Fozia Fozia − *Biochemistry Department, Khyber Medical University Institute of Medical Sciences, Kohat 26000, Pakistan;* orcid.org/0000-0002-4554-7427; Email: drfoziazeb@yahoo.com

Authors

Saeed M Aldossari − *Department of Clinical Laboratory Sciences, College of Applied Medical Sciences, King Saud University, Riyadh 11433, Saudi Arabia*

Latif Ur Rehman − *Department of Chemistry, Kohat University of Science & Technology, Kohat 26000, Pakistan*

Madeeha Aslam − *Department of Chemistry, Kohat University of Science & Technology, Kohat 26000, Pakistan*

Mohamed Mohany − *Department of Pharmacology and Toxicology, College of Pharmacy, King Saud University, Riyadh 11451, Saudi Arabia*

Marija Milošević − *Department of Biology and Ecology, Faculty of Science, University of Kragujevac, 34000 Kragujevac, Serbia*

Salim S. Al-Rejaie − *Department of Pharmacology and Toxicology, College of Pharmacy, King Saud University, Riyadh 11451, Saudi Arabia*

Mourad A. M. Aboul-Soud − *Department of Clinical Laboratory Sciences, College of Applied Medical Sciences, King Saud University, Riyadh 11433, Saudi Arabia*

Complete contact information is available at: https://pubs.acs.org/10.1021/acsomega.3c04484

Author Contributions

All authors participated in the design and interpretation of studies, data analysis, and manuscript review. L.U.R. and F.F. conducted the experiments and collected the data. I.A., M.A., and F.F. were responsible for the analysis and mapping of the data and provided methodological and technical guidance.

https://doi.org/10.1021/acsomega.3c04484
ACS Omega 2023, 8, 41214−41222

S.M.A. and L.U.R. wrote the manuscript, and M.Mo., M.Mi., S.S.A.-R., M.A.M.A.-S., F.F., M.A., and I.A. performed project administration and edited and reviewed the manuscript. All authors read and approved the final manuscript.

Notes

The authors declare no competing financial interest.
The Current study was approved by the ethical committee of the Department of Chemistry, Kohat University of Science & Technology, Kohat, Pakistan under the reference number KUST/EC/00823 dated 16/08/2022.
"Not applicable"

■ ACKNOWLEDGMENTS

The authors extend their appreciation to the Researchers Supporting Project (number RSPD2023R758), King Saud University, Riyadh, Saudi Arabia.

■ REFERENCES

(1) Zhang, H.-j.; Niu, X.-y.; Hu, J.; Ren, C.-l.; Chen, H.-l.; Chen, X.-g. Metallic nanoparticles immobilized in magnetic metal−organic frameworks: preparation and application as highly active, magnetically isolable and reusable catalysts. *Catal. Sci. Technol.* **2014**, *4* (9), 3013−3024.
(2) Wahajuddin; Arora, S. Superparamagnetic iron oxide nanoparticles: magnetic nanoplatforms as drug carriers. *Int. J. Nanomed.* **2012**, 3445−3471, DOI: 10.2147/IJN.S30320.
(3) Sun, Z.; Yathindranath, V.; Worden, M.; Thliveris, J. A.; Chu, S.; Parkinson, F. E.; Hegmann, T.; Miller, D. W. Characterization of cellular uptake and toxicity of aminosilane-coated iron oxide nanoparticles with different charges in central nervous system-relevant cell culture models. *Int. J. Nanomed.* **2013**, 961−970, DOI: 10.2147/IJN.S39048.
(4) Naqvi, S.; Samim, M.; Abdin, M.; Ahmed, F. J.; Maitra, A.; Prashant, C.; Dinda, A. K. RETRACTED ARTICLE: Concentration-dependent toxicity of iron oxide nanoparticles mediated by increased oxidative stress. *Int. J. Nanomed.* **2010**, 983−989, DOI: 10.2147/IJN.S13244.
(5) Rane, A. V.; Kanny, K.; Abitha, V.; Thomas, S. Methods for synthesis of nanoparticles and fabrication of nanocomposites. In *Synthesis of inorganic nanomaterials*; Elsevier, 2018; pp 121−139.
(6) Behravan, M.; Hossein Panahi, A.; Naghizadeh, A.; Ziaee, M.; Mahdavi, R.; Mirzapour, A. Facile green synthesis of silver nanoparticles using Berberis vulgaris leaf and root aqueous extract and its antibacterial activity. *Int. J. Biol. Macromol.* **2019**, *124*, 148−154.
(7) Yang, C.; Yan, H. A green and facile approach for synthesis of magnetite nanoparticles with tunable sizes and morphologies. *Mater. Lett.* **2012**, *73*, 129−132, DOI: 10.1016/j.matlet.2012.01.031.
(8) Salehiabar, M.; Nosrati, H.; Davaran, S.; Danafar, H.; Manjili, H. K. Facile Synthesis and Characterization of L-Aspartic Acid Coated Iron Oxide Magnetic Nanoparticles (IONPs) For Biomedical Applications. *Drug Res. (Stuttg)* **2018**, *68* (5), 280−285.
(9) Periakaruppan, R.; Kumar, T. S.; Vanathi, P.; Al-Awsi, G. R. L.; Al-Dayan, N.; Dhanasekaran, S. Phyto-synthesis and characterization of parthenium-mediated iron oxide nanoparticles and an evaluation of their antifungal and antioxidant activities and effect on seed germination. *JOM* **2023**, 1−8, DOI: 10.1007/s11837-023-05760-3.
(10) Ashraf, I.; Singh, N.; Agarwal, A. Green synthesis of iron oxide nanoparticles using Amla seed for methylene blue dye removal from water. *Mater. Today: Proc.* **2023**, *72*, 311−316, DOI: 10.1016/j.matpr.2022.07.404.
(11) Nadeem, F.; Fozia, F.; Aslam, M.; Ahmad, I.; Ahmad, S.; Ullah, R.; Almutairi, M. H.; Aleya, L.; Abdel-Daim, M. M. Characterization, Antiplasmodial and Cytotoxic Activities of Green Synthesized Iron Oxide Nanoparticles Using Nephrolepis exaltata Aqueous Extract. *Molecules* **2022**, *27* (15), 4931 DOI: 10.3390/molecules27154931.
(12) Kuzan, A. Toxicity of advanced glycation end products (Review). *Biomed. Rep.* **2021**, *14* (5), 1−8.
(13) Nguyen, H. P.; Katta, R. Sugar Sag: Glycation and the Role of Diet in Aging Skin. *Skin Ther. Lett.* **2015**, *20* (6), 1−5.
(14) Ahmed, N.; Thornalley, P. J. Quantitative screening of protein biomarkers of early glycation, advanced glycation, oxidation and nitrosation in cellular and extracellular proteins by tandem mass spectrometry multiple reaction monitoring. *Biochem. Soc. Trans.* **2003**, *31* (6), 1417−1422, DOI: 10.1042/bst0311417.
(15) Sutriyo, S.; Aripin, S. A. Antiglycation Effect Assay of Gold Nanoparticles Synthesized by Green Synthesis Method with Kacip Fatimah (Labisia pumila) Extract as Antiaging. In *Asian Federation for Pharmaceutical Sciences (AFPS) 2019*; 2019.
(16) Peron, S.; Hadi, F.; Azarbani, F.; Ananda Murthy, H. C. Antimicrobial, antioxidant, anti-glycation and toxicity studies on silver nanoparticles synthesized using Rosa damascena flower extract. *Green Chem. Lett. Rev.* **2021**, *14* (3), 519−533, DOI: 10.1080/17518253.2021.1963492.
(17) Anis, M.; Iqbal, M. Antipyretic utility of some Indian plants in traditional medicine. *Fitoterapia* **1986**, *57* (1), 52−55.
(18) Singh, A.; Lal, U. R.; Mukhtar, H. M.; Singh, P. S.; Shah, G.; Dhawan, R. K. Phytochemical profile of sugarcane and its potential health aspects. *Pharmacogn. Rev.* **2015**, *9* (17), 45 DOI: 10.4103/0973-7847.156340.
(19) Vedavathy, S.; Rao, K.; Rajaiah, M.; Nagaraju, N. Folklore information from Rayalaseema region, Andhra Pradesh for family planning and birth control. *Int. J. Pharmacogn.* **1991**, *29* (2), 113−116, DOI: 10.3109/13880209109082860.
(20) Akbarizadeh, M. R.; Naderifar, M.; Mousazadeh, F.; Zafarnia, N.; Sarani, M. Cytotoxic activity and Magnetic Behavior of green synthesized iron oxide nanoparticles on brain glioblastoma cells. *Nanomed. Res. J.* **2022**, *7* (1), 99−106, DOI: 10.22034/NMRJ.2022.01.010.
(21) Devi, H. S.; Boda, M. A.; Shah, M. A.; Parveen, S.; Wani, A. H. Green synthesis of iron oxide nanoparticles using Platanus orientalis leaf extract for antifungal activity. *Green Process. Synth.* **2019**, *8* (1), 38−45, DOI: 10.1515/gps-2017-0145.
(22) Yardily, A.; Sunitha, N. Green synthesis of iron nanoparticles using hibiscus leaf extract, characterization, antimicrobial activity. In *International Journal of Scientific Research and Revie*; **2019**, *8* (7).
(23) Miri, A.; Najafzadeh, H.; Darroudi, M.; Miri, M. J.; Kouhbanani, M. A. J.; Sarani, M. Iron oxide nanoparticles: biosynthesis, magnetic behavior, cytotoxic effect. *ChemistryOpen* **2021**, *10* (3), 327−333, DOI: 10.1002/open.202000186.
(24) Saravanan, A.; Kumar, P. S.; Varjani, S.; Karishma, S.; Jeevanantham, S.; Yaashikaa, P. J. Effective removal of Cr (VI) ions from synthetic solution using mixed biomasses: kinetic, equilibrium and thermodynamic study. *J. Water Process Eng.* **2021**, *40*, No. 101905, DOI: 10.1016/j.jwpe.2020.101905.
(25) Mahdavi, M.; Namvar, F.; Ahmad, M. B.; Mohamad, R. Green biosynthesis and characterization of magnetic iron oxide (Fe3O4) nanoparticles using seaweed (Sargassum muticum) aqueous extract. *Molecules* **2013**, *18* (5), 5954−5964, DOI: 10.3390/molecules18055954.
(26) Arakha, M.; Pal, S.; Samantarrai, D.; Panigrahi, T. K.; Mallick, B. C.; Pramanik, K.; Mallick, B.; Jha, S. Antimicrobial activity of iron oxide nanoparticle upon modulation of nanoparticle-bacteria interface. *Sci. Rep.* **2015**, *5* (1), 14813 DOI: 10.1038/srep14813.
(27) Venkateswarlu, S.; Kumar, B. N.; Prasad, C.; Venkateswarlu, P.; Jyothi, N. Bio-inspired green synthesis of Fe3O4 spherical magnetic nanoparticles using Syzygium cumini seed extract. *Phys. B* **2014**, *449*, 67−71, DOI: 10.1016/j.physb.2014.04.031.
(28) Bhuiyan, M. S. H.; Miah, M. Y.; Paul, S. C.; Aka, T. D.; Saha, O.; Rahaman, M. M.; Sharif, M. J. I.; Habiba, O.; Ashaduzzaman, M. Green synthesis of iron oxide nanoparticle using Carica papaya leaf extract: application for photocatalytic degradation of remazol yellow RR dye and antibacterial activity. *Heliyon* **2020**, *6* (8), No. e04603, DOI: 10.1016/j.heliyon.2020.e04603.

(29) Behera, S. S.; Patra, J. K.; Pramanik, K.; Panda, N.; Thatoi, H. Characterization and evaluation of antibacterial activities of chemically synthesized iron oxide nanoparticles. 2012. DOI: 10.4236/wjnse.2012.24026
(30) Kuang, Y.; Wang, Q.; Chen, Z.; Megharaj, M.; Naidu, R. Heterogeneous Fenton-like oxidation of monochlorobenzene using green synthesis of iron nanoparticles. *J. Colloid Interface Sci.* **2013**, *410*, 67−73.
(31) Bharathi, D.; Preethi, S.; Abarna, K.; Nithyasri, M.; Kishore, P.; Deepika, K. Bio-inspired synthesis of flower shaped iron oxide nanoparticles (FeONPs) using phytochemicals of Solanum lycopersicum leaf extract for biomedical applications. *Biocatal. Agric. Biotechnol.* **2020**, *27*, No. 101698.
(32) Abdallah, R. M.; Al-Haddad, R. M. Optical and Morphology Properties of the Magnetite (Fe3O4) Nanoparticles Prepared by Green Method. In *Journal of Physics: Conference Series, 2021*; IOP Publishing: Vol. 1829; p 012022.
(33) Abd Al-hameed, S.; Mohammed, A. M. Novel green synthesis of Fe2O3 nanoparticles using persimmon extract and study their anticancer and anti-bacterial activity. *J. Pharm. Negat. Results* **2022**, *13* (3), 958−967.
(34) Zahid, K.; Ahmed, M.; Khan, F. Phytochemical screening, antioxidant activity, total phenolic and total flavonoid contents of seven local varieties of Rosa indica L. *Nat. Prod. Res.* **2018**, *32* (10), 1239−1243.
(35) Singh, J.; Dutta, T.; Kim, K.-H.; Rawat, M.; Samddar, P.; Kumar, P. 'Green'synthesis of metals and their oxide nanoparticles: applications for environmental remediation. *J. Nanobiotechnol.* **2018**, *16* (1), 1−24.
(36) GhoshMoulick, R.; Bhattacharya, J.; Mitra, C. K.; Basak, S.; Dasgupta, A. K. J. N. N. Medicine. Protein seeding of gold nanoparticles and mechanism of glycation sensing. *Biology* **2007**, *3* (3), 208−214.
(37) GhoshMoulick, R.; Bhattacharya, J.; Roy, S.; Basak, S.; Dasgupta, A. K. Compensatory secondary structure alterations in protein glycation. *Proteomics* **2007**, *1774* (2), 233−242.
(38) Peng, X.; Ma, J.; Chen, F.; Wang, M. Naturally occurring inhibitors against the formation of advanced glycation end-products. *Food Funct.* **2011**, *2* (6), 289−301.
(39) Ankamwar, B.; Lai, T.; Huang, J.; Liu, R.; Hsiao, M.; Chen, C.; Hwu, Y. J. N. Biocompatibility of Fe3O4 nanoparticles evaluated by in vitro cytotoxicity assays using normal, glia and breast cancer cells. *Nanotechnology* **2010**, *21* (7), No. 075102, DOI: 10.1088/0957-4484/21/7/075102.
(40) Izadiyan, Z.; Shameli, K.; Miyake, M.; Hara, H.; Mohamad, S. E. B.; Kalantari, K.; Taib, S. H. M.; Rasouli, E. Cytotoxicity assay of plant-mediated synthesized iron oxide nanoparticles using Juglans regia green husk extract. *Arabian J. Chem.* **2020**, *13* (1), 2011−2023, DOI: 10.1016/j.arabjc.2018.02.019.
(41) Arias, L. S.; Pessan, J. P.; Vieira, A. P. M.; Lima, T. M. T. d.; Delbem, A. C. B.; Monteiro, D. R. Iron oxide nanoparticles for biomedical applications: A perspective on synthesis, drugs, antimicrobial activity, and toxicity. *Antibiotics* **2018**, *7* (2), 46 DOI: 10.3390/antibiotics7020046.

https://doi.org/10.1021/acsomega.3c04484
ACS Omega 2023, 8, 41214−41222